第 49 卷第 3 期　　硅　酸　盐　学　报　　Vol. 49，No. 3
2021 年 3 月　　JOURNAL OF THE CHINESE CERAMIC SOCIETY　　March，2021
http://www.gxyb.cbpt.cnki.net　　DOI：10.14062/j.issn.0454-5648.20200461

TiB_2 对无压烧结 B_4C–TiB_2 复相陶瓷结构和性能的影响

李宗家[1]，程焕武[1,2]，王扬卫[1,2]，朱　宇[1]，安　瑞[1]，方海燕[1]，艾丽菲亚[1]

(1. 北京理工大学材料学院，北京 100081；2. 冲击环境下材料技术重点实验室，北京 100081)

摘　要：以碳化硼(B_4C)、二硼化钛(TiB_2)、碳化钛(TiC)为原料，采用无压烧结法在 2 130 ℃制备了含 20% (质量分数)和 30%TiB_2 的 B_4C 基复相陶瓷，分析所制样品的密度、硬度、弯曲强度和断裂韧性。结果表明：在 2 130 ℃，直接加入 30%的 TiB_2 亚微米颗粒，复相陶瓷的抗弯强度和断裂韧性分别达到 277.6 MPa 和 5.38 MPa·$m^{1/2}$。陶瓷中颗粒拔出和裂纹微桥接对复相陶瓷增韧作用显著。B_4C–TiB_2 复相陶瓷的增韧机理主要是由于 TiB_2 与 B_4C 热膨胀系数不匹配产生的残余应力导致的微裂纹增韧和裂纹偏转增韧。

关键词：无压烧结；碳化硼–硼化钛复相陶瓷；微观结构；力学性能
中图分类号：TQ174　　**文献标志码：**A　　**文章编号：**0454–5648(2021)03–0461–08
网络出版时间：2021–01–21



Effects of TiB_2 on Microstructure and Mechanical Properties of Pressure-less-sintered B_4C–TiB_2 Composites

LI Zongjia[1], *CHENG Huanwu*[1,2], *WANG Yangwei*[1,2], *ZHU Yu*[1], *AN Rui*[1], *FANG Haiyan*[1], *AILI Feiya*[1]
(1. School of Material Science and Engineering, Beijing Institute of Technology, Beijing 100081, China; 2. National Key Laboratory of Science and Technology on Materials under Shock and Impact, Beijing Institute of Technology, Beijing 100081, China)

Abstract: Boron carbide matrix composites containing boron carbide (B_4C), titanium diboride (TiB_2) at 20% (mass fraction) and 30%, and titanium carbide (TiC) were fabricated at 2 130 ℃ using a pressure-less sintering method. Different amounts of TiB_2 and TiC particles were added to B_4C. TiB_2 content was chosen as the main variable to study the effect on the composites. The density, hardness, bending strengths and fracture toughness measurements were performed to obtain the physical and mechanical properties of the samples. The results indicate that by adding 30%TiB_2 sub-micron particles at 2 130 ℃, the bending strength and fracture toughness of 277.6 MPa and 5.38 MPa·$m^{1/2}$ were obtained for the composite. Particle pullout and crack micro-bridging play an effective role in toughening the composite ceramics. The main toughening mechanisms of the B_4C–TiB_2 composites are noted to possess microcrack and crack deflection toughening owing to the residual stresses resulting from the mismatch of the thermal expansion coefficient between TiB_2 and B_4C.

Keywords: pressure-less sintering; boron carbide–titanium diboride composites; microstructure; mechanical properties

1　Introduction

Due to its low density in addition to its high hardness and melting point, boron carbide (B_4C) is widely used for lightweight armor and cutting tools. B_4C belongs to the group of non-metallic hard materials with hardness that is only inferior to diamond and cubic boron nitride[1]. However, the poor toughness and sintering performance of B_4C hinder its application to some extent[2–5].

Efforts have been made to enhance the sintering capabilities and mechanical properties of B_4C. Compared to sintering methods, such as hot pressing and spark plasma sintering, pressure-less sintering is a relatively simple and economical method that can be used for the preparation of large and complex parts[6].

收稿日期：2019–06–28。　修订日期：2019–07–28。
第一作者：李宗家(1995—)，男，硕士研究生。
通信作者：程焕武(1967—)，男，副研究员。

Received date: 2019–06–28.　**Revised date:** 2019–07–28.
First author: LI Zongjia (1995–), male, Master candidate.
E-mail: zongjial@126.com
Corresponding author: CHENG Huanwu (1967–), male, Ph.D., associate Professor.
E-mail: chenghuanwu@bit.edu.cn

Furthermore, many additives are incorporated into B_4C to improve its ceramic properties, and the results have shown that TiB_2 is an ideal choice as an additive for the B_4C matrix[7–10]. According to literature studies, two main methods for adding TiB_2 to the B_4C ceramics are used. One involves the direct addition of TiB_2 particles[11], and the other is based on the chemical reaction of B_4C with additives such as Ti[12–13], TiO_2[9], and TiC[14–15], indicating an *in-situ* method to prepare TiB_2. The addition of TiC can effectively improve the properties of B_4C, and the studies show that TiC reacts with B_4C to form TiB_2 in the system according to the following reaction. However, in B_4C–TiB_2 composite research aspects, most studies have focused on reactive hot-pressing, while few studies have focused on direct addition of TiB_2 or the reaction with that leads to formation of TiB_2 *via* the easy and cheap pressure-less sintered method. Large-scale industrial production of ceramics is hampered by the high economic and poor efficiency costs of hot-pressing.

$$2TiC+B_4C \rightarrow 2TiB_2+3C$$

Extensive studies on improving the toughness of B_4C ceramics by combining the addition of TiB_2 particles and pressure-less sintering are necessary. Few studies have explored the different effects of directly added or B_4C–TiC reaction that forms TiB_2 on B_4C using the pressure-less sintering method based on the corresponding impact on the microstructure and mechanical properties. What remains unclear about the toughening mechanism is whether the two methods of forming TiB_2 facilitate each other or only one method actually plays a major role during the synthesis. In this study, the influence of TiB_2 addition on the microstructure and mechanical properties of pressure-less sintered B_4C–TiB_2 composites at 2 130 ℃ has been investigated. The different addition methods were evaluated by comparing the corresponding impact on the microstructure and mechanical properties of the B_4C–TiB_2 composites, such as their densities, hardness, bending strengths, and fracture toughness.

2 Experimental

Commercially available B_4C powder (~3.19 μm, Zhengzhou Songshan Material Co., China), TiC powder (about 5.02 μm, Shanghai Shuitian Material Co., China), and TiB_2 powder (about 0.20 μm, Shanghai Shuitian Material Co., China) were used as raw starting materials. Si powder (about 2.40 μm, Shanghai Shuitian Material Co., China) and C powder (about 0.50 μm, Shanghai Shuitian Material Co., China) were used as sintering aids since previous results have shown that C and Si are effective sintering aids for improving the sintering capabilities and mechanical properties[16]. The purity of all raw material powders was greater than 99%. The powder mixtures of six different compositions were prepared by wet ball-milling at 200 r/min for 12 h in a polyethylene bottle, using zirconium oxide (ZrO_2) balls and alcohol medium. The mass ratio of the balls to powders was 3:1. The mixtures were dried in a rotary evaporator followed by crushing and screening through a 100-mesh sieve. Afterwards, green compacts were formed by uniaxial pressing at about 50 MPa, followed by cold isostatic pressing at 200 MPa and sintering using a graphite element vacuum furnace at 2 130 ℃ for 40 min. The initial heating rate was 6–8 ℃/min. After reaching 1 800 ℃, the heating rate was enhanced to 9–10 ℃/min. The temperature was maintained for 40 min. It was followed by cooling at a rate of 9 to 11 ℃/min. After cooling down to 500 ℃, the materials and furnace were then slowly cooled. The sintering process curve is shown in Fig. 1.

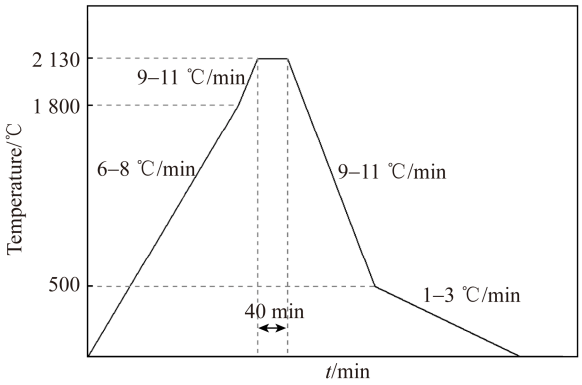


Fig. 1 Sintering process curve

Table 1 Composition and nomenclature of the powder mixture *w*/%

Designation	B_4C	TiC	TiB_2	C	Si
80B_4C–10TiC	80	10	0	7	3
70B_4C–20TiB_2	70		20	7	3
70B_4C–6.67TiC–13.33TiB_2	70	6.67	13.33	7	3
70B_4C–20TiC	70	20	0	7	3
60B_4C–30TiB_2	60		30	7	3
60B_4C–10TiC-20TiB_2	60	10	20	7	3

w—Mass fraction.

The samples were polished, and density values were measured using the standard Archimedes' method. Bending strength and fracture toughness (K_{IC}) were measured on a universal testing machine (INSTRON-5985, Norwood, America). The three-point bending test with a span of 30 mm and a loading rate of 0.5 mm/min was conducted on the specimens (36.0 mm×3.0 mm×4.0 mm) to evaluate the bending strength; the single-edge notched beam method with a span of 30 mm and a loading rate of 0.05 mm/min was used on the specimens (36.0 mm×3.0 mm×6.0 mm) to measure the fracture toughness. The bending strength

and the fracture toughness values were determined from the results averaged from seven bars. Crystalline phases in the sintered specimens were performed using CuKα (λ=0.154 nm) radiation with X-ray diffraction (XRD, Ultima III, Rigaku, Japan), and the data were collected at a scan rate of 0.02(°)/s for 2θ varying from 10° to 80°. Microstructure and compositional analyses were examined *via* scanning electron microscopy (SEM, Hitachi-S3400N, Japan).

3 Results and discussion

3.1 Phase transition process

Fig. 2 shows the XRD patterns of the as-mixed $B_4C/TiB_2/TiC/Si/C$ composite powders. As expected, B_4C and TiB_2 are the main crystalline phases in all powder samples. Si that reacted with C powder or C element in the B_4C matrix to form an SiC phase as detected on the XRD pattern. Furthermore, it could be observed that the TiC phase disappeared, which indicated that the occurred during the sintering of the ceramic samples and the TiC phase reacted completely. This finding suggests that the main effect on the microstructure and properties of the multiphase ceramics was the presence of TiB_2 as the second phase for the pre-designed three- or two-phase ceramic systems. The diffraction peak intensities of TiB_2 in B_4C–30%TiB_2 were enhanced in comparison to those of B_4C–20%TiB_2, which indicates that the TiB_2 content in B_4C–30%TiB_2 is higher than that in B_4C–20%TiB_2. The TiB_2 diffraction peak strength of the composite ceramics prepared by direct addition of TiB_2 was higher than that of the other two methods in the same group.

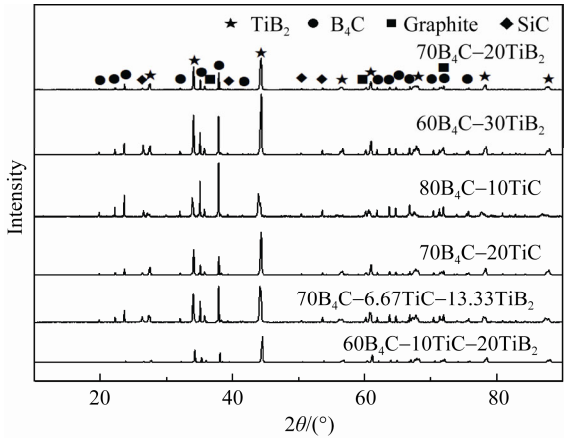


Fig. 2　XRD patterns of composites

3.2 Microstructure

The backscattered electron (BSE) images of the polished B_4C–TiB_2 composites are shown in Fig. 3. It can be seen that the B_4C–TiB_2 composites consisted of three phases: (1) the dark areas represent the B_4C phase, (2) the bright areas are the TiB_2 phase, and (3) the gray areas represent the SiC phase. The SiC phase with small size is noted to be dispersed in the B_4C matrix and presents a plate-like tissue morphology with a large aspect ratio, thus, helping to improve the mechanical properties of the whisker-toughened ceramic. A small amount of laminated (white-dotted bordered rectangle) and flocculated (black-dottedbordered rectangle) graphite phase can also be seen in Fig. 4. Generally, there are two sources of the

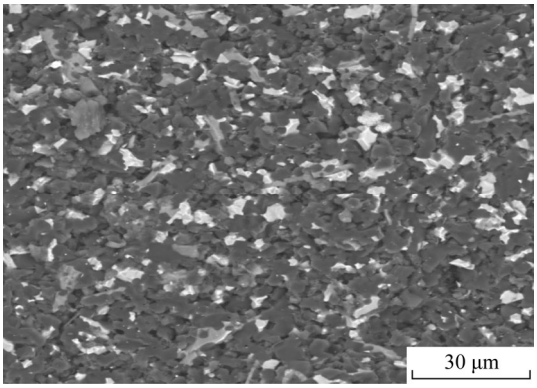
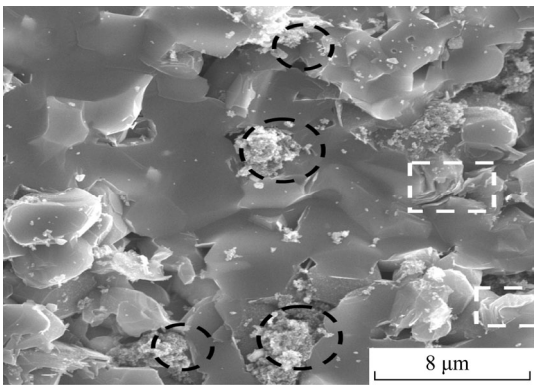
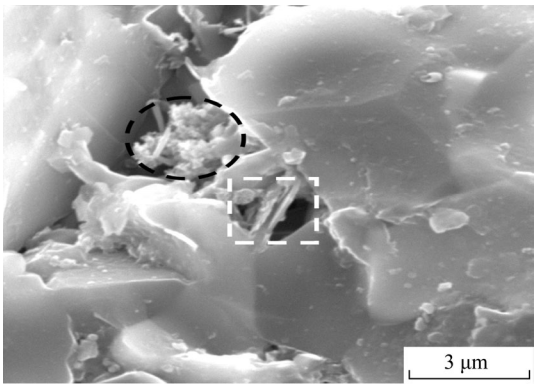


Fig. 3　Backscattered electron (BSE) images of boron carbide–titanium boride (B_4C–TiB_2) composites



(a) $70B_4C$–$20TiB_2$



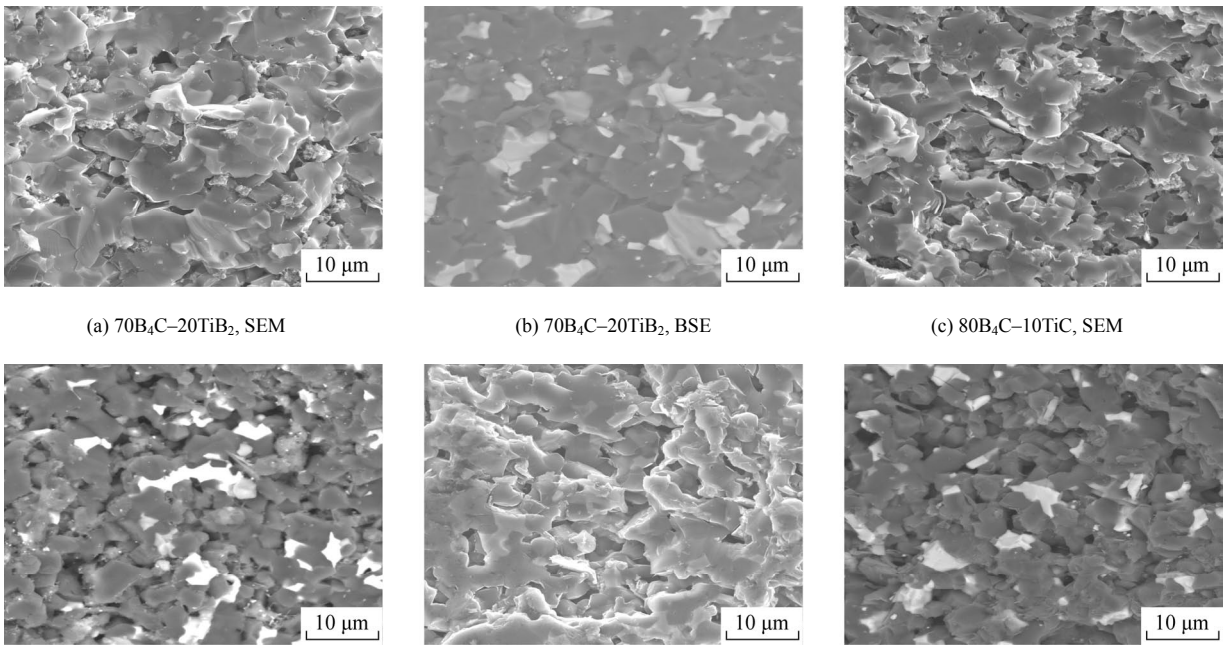
(b) $60B_4C$–$30TiB_2$

White dotted bordered rectangle indicates laminated graphite phase and the black-dotted bordered rectangle indicates flocculated graphite phase.

Fig. 4　SEM images of graphite phase in B_4C–TiB_2 composites

graphite phase. In the first case, finely dispersed TiB_2 and graphite phases were formed by the reaction of B_4C with TiC during pressure-less sintering, which were observed to be closely bound to the matrix. In the second case, the C particles used as a sintering aid are graphitized at high temperatures, thus, forming the graphite phase. The graphite grains promoted the sintering rate as graphite located on the grain boundary inhibited the grain growth and caused an increase in the grain boundary quantity, thereby, increasing the material transport between the adjacent B_4C grains, and thus, promoting sintering. The graphite phase in the matrix appears to have absorbed the energy of the crack propagation by torsion, deflection, and fracture under the action of the external forces. Furthermore, the crack propagation direction appears to have been made perpendicular to the laminated graphite direction to further hinder the crack propagation.

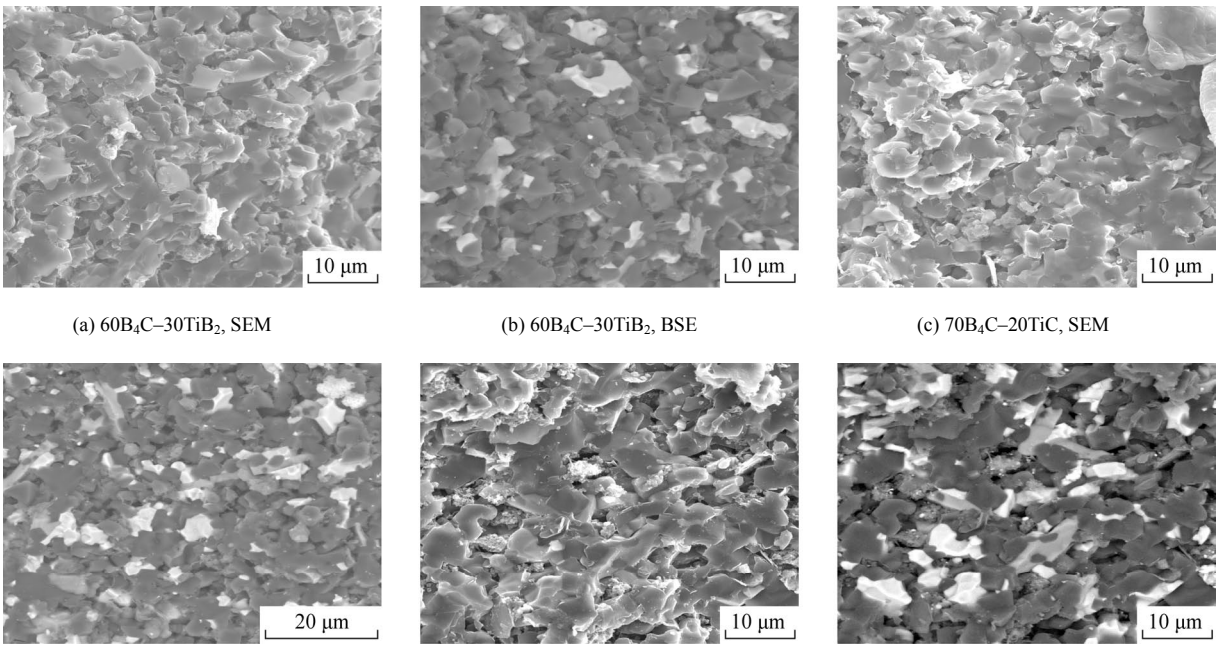
Fig. 5 and Fig. 6 show the secondary electron and BSE fracture images of the composites of B_4C–20%TiB_2 and B_4C–30%TiB_2, respectively. The porosity was observed in all samples, and the density differences between B_4C–20%TiB_2 and B_4C–30%TiB_2 were not significant as shown in the figure. The agglomerated graphite filling in the pores of the ceramic matrix is commonly observed to enhance the densification. A few sharp sintering concave necks can be noted in Fig. 5(a), which also confirms the reason for the low relative density of $80B_4C$–10TiC as shown in Fig. 9(a). The more round the sintering neck, the fuller the sintering and the higher the sintering density was. A few regional neck growths were noted to increase and develop into a three-dimensional (3D) interpenetrating network of particles, thus, leading to further increase in the degree of densification in $70B_4C$–$20TiB_2$ and $70B_4C$–6.67TiC–13.33TiB_2. The pores were observed to open and become interconnected to facilitate the gas discharge in the sintering process. Thus, the microstructure of $70B_4C$–$20TiB_2$ developed more obviously along with further densification to 98.86%. Similar phenomena were observed to occur for B_4C–30%TiB_2 materials as shown in Fig. 6. The sintering necks of the three samples grew with $70B_4C$–20TiC and $60B_4C$–$30TiB_2$ and exhibited a higher degree of growth and fewer pores. Hence, the densification of $70B_4C$–20TiC and $60B_4C$–$30TiB_2$ was relatively higher in B_4C–30%TiB_2 with a relative density of 97.63% and 94.91%, respectively, as shown in Fig. 9(a). It can be seen in Fig. 6(d) that the TiB_2 particles were finer and more evenly distributed than those in Fig. 6(b) and (f). The fine microstructure led to high mechanical properties due to the Hall–Petch effect, whereas the evenly distributed particles could effectively toughen the composite ceramics, thus, resulting in optimal mechanical properties for the $60B_4C$–$30TiB_2$ composite. Comparing the SE images with the corresponding BSE images, it can be seen that the fracture mode of B_4C is noted to be mainly transgranular, whereas it is mainly intergranular for TiB_2. The mixed fracture mode appears to be favorable for the toughness of the B_4C–TiB_2 composites as also reported in literature[8–9].



(a) $70B_4C$–$20TiB_2$, SEM (b) $70B_4C$–$20TiB_2$, BSE (c) $80B_4C$–10TiC, SEM

(d) $80B_4C$–10TiC, BSE (e) $60B_4C$–6.67TiC–13.33TiB_2, SEM (f) $60B_4C$–6.67TiC–13.33TiB_2, BSE

Fig. 5 SEM and BSE images of the fracture composites of B_4C–20%TiB_2



(a) $60B_4C$–$30TiB_2$, SEM　(b) $60B_4C$–$30TiB_2$, BSE　(c) $70B_4C$–$20TiC$, SEM

(d) $70B_4C$–$20TiC$, BSE　(e) $60B_4C$–$10TiC$–$20TiB_2$, SEM　(f) $60B_4C$–$10TiC$–$20TiB_2$, BSE

Fig. 6　SEM images of the fracture composites of B_4C–30%TiB_2

Fig. 7 shows the crack growth path of the B_4C–TiB_2 composite. It is obvious that numerous crack deflections occurred during the crack propagation process, and the large angle crack deflection (blue dotted bordered rectangle) occurred in the two-phase junction region. Also, crack micro-bridging (red-dotted bordered rectangle) was observed, and the results indicate that it could improve the fracture toughness of the ceramics. Most of the cracks were observed to grow around the microcrack and pores (white-dotted bordered rectangle). Besides, the grains deflected the cracks (black-dotted-bordered rectangle); thus, the fracture mode changed from the transgranular to the intergranular fracture followed by switching back to the transgranular fracture after the crack moved around the grain. The phenomenon of crack branching can also be noted in the upper left corner of Fig. 7. As the main crack leading to the fracture expanded, evenly distributed microcracks due to the different thermal expansion coefficients of the ceramic matrix and second phase will promote bifurcation of the main crack, thus, making the path of the main crack tortuous and uneven. It caused an increase in the surface energy during the expansion process, thus, hindering the rapid crack expansion and enhancing the toughness of the material, which are the fundamental reasons for the microcrack toughening. Both microcrack and crack deflection toughening resulted from the residual stresses caused by the mismatch in the thermal expansion coefficient of TiB_2 and B_4C.

Fig. 8 shows the phenomenon of the particle pullout, and a hexagonal pit 0.5 μm wide and 1 μm long could be observed. The particle pullout is a typical feature of the intergranular fracture, which can consume a large amount of crack energy, thus, improving the toughness of the composites. Overall, the crack deflection, particle pullout, crack micro-bridging, microcrack toughening, and mixed fracture mode are effective means for improving ceramic toughness. On the other hand, the thermal expansion coefficient difference between particle and ceramic matrices was the main factor determining the toughening effect.

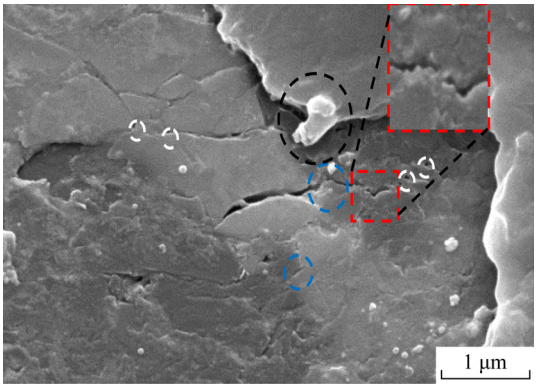
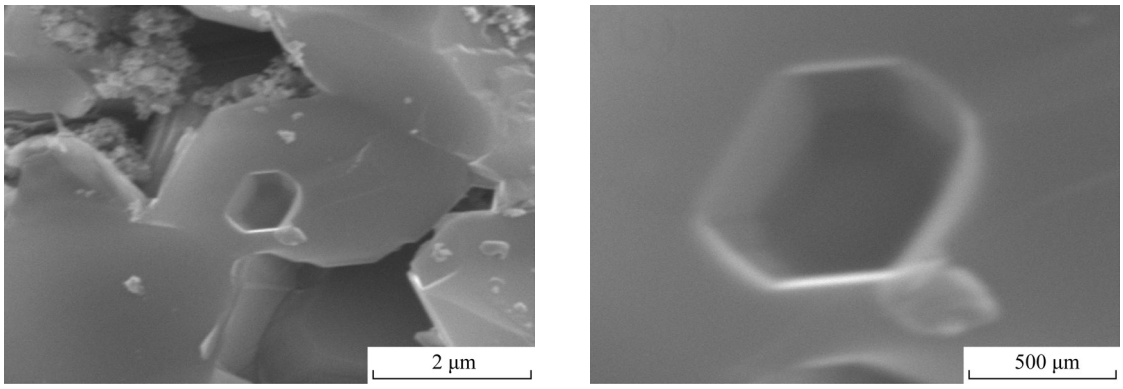


Fig. 7　SEM images of the crack propagations

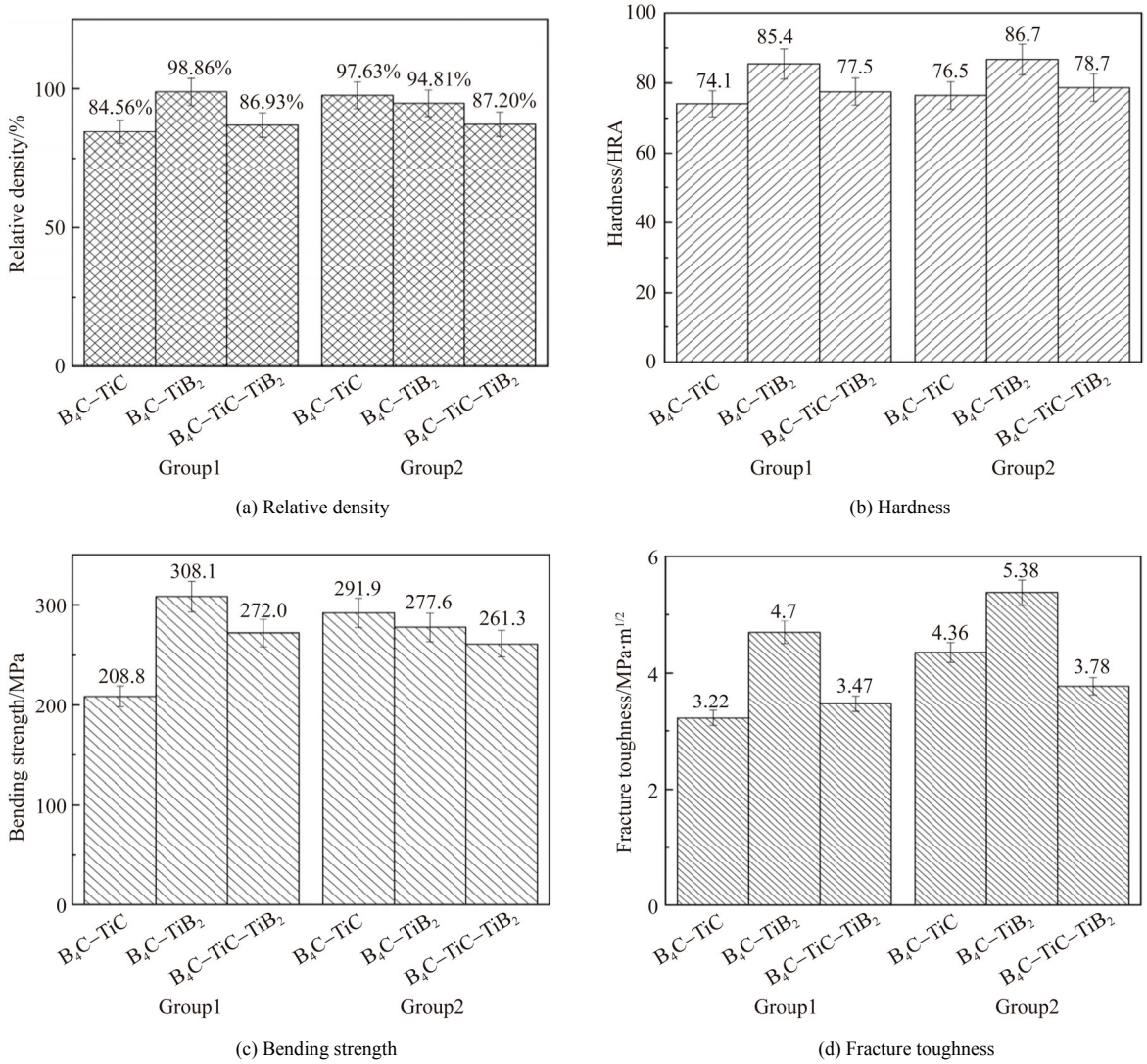
3.3　Mechanical properties

The relative density, Rockwell hardness, bending strength and fracture toughness of B_4C–20%TiB_2 and B_4C–30%TiB_2 are shown in Fig. 9. It can be observed that the comprehensive mechanical properties of B_4C–30%TiB_2 were better than B_4C–20%TiB_2, indicating that the composites containing 30%TiB_2 exhibited a superior mechanical performance over the



(a) Particle pullout (b) Partial enlarged view

Fig. 8 SEM images of the particle pullout and partial enlarged view



(a) Relative density (b) Hardness

(c) Bending strength (d) Fracture toughness

Fig. 9 Mechanical properties of as-prepared B_4C–TiB_2 composites

composites containing 20%TiB_2. This finding could be attributed to an increase in the thermal expansion coefficient of the composite with the amount of TiB_2. Specifically, Fig. 9(a) shows the relative densities of the composites. Compared to the other two components in B_4C–20%TiB_2, the maximum value is noted to be 98.86% for 70B_4C–20TiB_2. It indicates that the sintering of the B_4C–20%TiB_2 composite at 2 130 ℃ leads to high density in the case of direct addition of the B_4C powder rather than the addition of

TiC or TiC and B_4C mixed powders. In short, the effect of direct addition of TiB_2 to the composite ceramics to improve the relative density of the ceramics is observed to the most effective strategy. Similar to B_4C–20%TiB_2, the ceramic sintered with the 70B_4C–20TiC components exhibited the highest densification in B_4C–30%TiB_2 with a value of 97.63%. Thus, in terms of the relative density of the B_4C–30%TiB_2 component, direct addition of the TiC powder was more effective as compared to the addition of B_4C or TiC and B_4C mixed powders. In other words, TiB_2 generated by the *in-situ* reaction of TiC in the B_4C–30%TiB_2 system improved the sinterability of the composite ceramics effectively. Fig. 9(b) shows the Rockwell hardness of the sintered samples. 70B_4C–20TiB_2 and 60B_4C–30TiB_2 exhibited the highest hardness of 85.4 HRA and 86.7 HRA in each group, respectively. This finding indicates that the TiB_2 particles played a key role in the hardness of the B_4C–TiB_2 composite ceramics. Moreover, compared to the reaction of TiC with B_4C to form TiB_2, it was found that TiB_2, as the second phase directly added to the composites, could improve the ceramic hardness more effectively. Hence, the hardness of the composites sintered with the pre-designed B_4C–TiC–TiB_2 component was higher than the composites sintered with the B_4C–TiC component.

The bending strength and fracture toughness of the materials are shown in Figs. 9(c) and 9(d), respectively. Compared with the monolithic B_4C ceramics, the toughness of the B_4C–TiB_2 ceramic composites was greatly improved due to the presence of TiB_2. The difference in the bending strength was noted to be consistent with the change in the relative density. Generally, low densification is one of the reasons for the reduction in the bending strength as the stress concentration tends to occur near the pores, which leads to the material failure after critical value is reached. The maximum bending strength among the B_4C–20%TiB_2 materials was noted for 70B_4C–20TiB_2, whereas the maximum bending strength in B_4C–30% TiB_2 was observed for 70B_4C–20TiC with values of 308.1 MPa and 291.9 MPa, respectively. The maximum fracture toughness of the B_4C–TiB_2 composites in this study was observed to be 5.38 MPa·$m^{1/2}$, which was more than twice the values reported for the monolithic B_4C ceramics (2.4–2.6 MPa·$m^{1/2}$)[Speyer R F, Lee H. Advances in pressureless densification of boron carbide[J]. J Mater Sci, 2004, 39(19): 6017–6021.[7]], rarely observed for the pressure-less sintered B_4C ceramics. Moreover, the fracture toughness of 70B_4C–20TiB_2 and 60B_4C–30TiB_2 was much higher than the other two in the group, and the material with the lowest fracture toughness among the samples had a higher toughness than the monolithic B_4C ceramics. This finding indicates that the addition of the TiB_2 particles could effectively improve the fracture toughness of the B_4C–TiB_2 composite ceramics, and the effect of the direct addition of TiB_2 particles is the most prominent. By comparing the mechanical properties of the samples, it could be observed that the two-phase system had superior properties compared to the three-phase system with optimal comprehensive properties achieved by the direct addition of TiB_2. Also, the addition of TiB_2 or the incorporation of TiC into the B_4C ceramics to form TiB_2 as the second phase represented two completely different principles. The results proved that the two methods of forming TiB_2 did not facilitate each other, and only one method played a major role during the synthesis. Moreover, direct addition of TiB_2 exhibited a more important role than the use of TiC to form TiB_2; however, this phenomenon is dependent on the reaction conditions, such as the particle size, sintering temperature, sintering holding time, and other conditions that have an impact on the experimental results.

4 Conclusions

The effect of TiB_2 addition methods on the microstructure and mechanical properties of the pressure-less sintered B_4C–TiB_2 composites at 2 130 ℃ was investigated. The results indicate that the mechanical properties of the two-phase system are better than the three-phase system. Moreover, direct addition of the TiB_2 powder is noted to be better than the addition of TiC or TiB_2 and TiC mixed powders in terms of the overall mechanical properties. The B_4C–TiB_2 composites with 30%TiB_2 added directly exhibited optimal performance, with relative density, hardness, bending strength, and fracture toughness values of 94.81%, 86.71 HRA, 277.6 MPa, and 5.38 MPa·$m^{1/2}$, respectively. The toughening mechanisms were found to be microcrack deflection, particle pullout, and crack micro-bridging.

References:

[1] HEYDARI M S, BAHARVANDI H R, DOLATKHAH K. Effect of TiO_2 nanoparticles on the pressureless sintering of B_4C–TiB_2 nanocomposites[J]. Intern J Refr Metals Hard Mater, 2015, 51: 6–13.

[2] HE Q, XIE J, WANG A, et al. Effects of boron content on the microstructures and mechanical properties of reactive hot–pressed B_xC–TiB_2–SiC composites[J]. Ceram Inter, 19, 45(16): 19650–19657.

[3] THÉVENOT F. Boron carbide—A comprehensive review[J]. J Eur Ceram Soc, 1990, 6(4): 205–225.

[4] DOMNICH V, REYNAUD S, HABER R A, et al. Boron carbide: structure, properties, and stability under stress[J]. J Am Ceram Soc, 2011, 94(11): 3605–3628.

[5] MOSKOVSKIKH D O, PARAMONOV K A, NEPAPUSHEV A A, et al. Bulk boron carbide nanostructured ceramics by reactive spark plasma sintering[J]. Ceram Inter, 2017, 43(11): 8190–8194.

[6] SPEYER R F, LEE H. Advances in pressureless densification of boron carbide[J]. J Mater Sci, 2004, 39(19): 6017–6021.

[7] YAMADA S, HIRAO K, YAMAUCHI Y, et al. High strength B_4C–TiB_2 composites fabricated by reaction hot-pressing[J]. J Eur

Ceram Soc, 2003, 23(7): 1123–1130.

[8] YUE X, ZHAO S, LÜ P, et al. Synthesis and properties of hot pressed B_4C–TiB_2 ceramic composite[J]. Mater Sci Eng: A, 2010, 527(27/28): 7215–7219.

[9] HUANG S G, VANMEENSEL K, VAN der Biest O, et al. *In situ* synthesis and densification of submicrometer-grained B_4C–TiB_2 composites by pulsed electric current sintering[J]. J Eur Ceram Soc, 2011, 31(4): 637–644.

[10] WANG Y, PENG H, YE F, et al. Effect of TiB_2 content on microstructure and mechanical properties of *in-situ* fabricated TiB_2/B_4C composites[J]. Transact Nonferr Metals Soc China, 2011, 21: s369–s373.

[11] SRIVATSAN T S, GURUPRASAD G, BLACK D, et al. Influence of TiB_2 content on microstructure and hardness of TiB_2–B_4C composite[J]. Powder Technol, 2005, 159(3): 161–167.

[12] CUI H, LIU W, CAO L, et al. Effects of B_4C particle size on pore structures of porous TiB_2–TiC by reaction synthesis[J]. J Eur Ceram Soc, 2015, 35(13): 3381–3388.

[13] WANG H, SUN S, WANG D, et al. Characterization of the structure of TiB_2/TiC composites prepared via mechanical alloying and subsequent pressureless sintering[J]. Powder Technol, 2012, 217: 340–346.

[14] POPOV O, VISHNYAKOV V, CHORNOBUK S, et al. Mechanisms of TiB_2 and graphite nucleation during TiC–B_4C high temperature interaction[J]. Ceram Inter, 2019, 45(14): 16740–16747.

[15] ZHANG X, ZHANG Z, LIU Y, et al. High-performance B_4C–TiB_2–SiC composites with tuneable properties fabricated by reactive hot pressing[J]. J Eur Ceram Soc, 2019, 39(10): 2995–3002.

[16] REHMAN S S, JI W, KHAN S A, et al. Microstructure and mechanical properties of B_4C densified by spark plasma sintering with Si as a sintering aid[J]. Ceram Inter, 2015, 41(1): 1903–1906.